UNIVERSITYOF BIRMINGHAM

The Relationship between Model Biases in East Asian Summer Monsoon Rainfall and Land Evaporation

Geen, Ruth; Pietschnig, Marianne; Agrawal, Shubhi; Dey, Dipanjan; Lambert, F. Hugo; Vallis, Geoffrey K.

[Link to publication on Research at Birmingham portal](#)

• Original Paper •

The Relationship between Model Biases in East Asian Summer Monsoon Rainfall and Land Evaporation※

Ruth GEEN[*1,2], Marianne PIETSCHNIG[2], Shubhi AGRAWAL[3,2], Dipanjan DEY[4,2],
F. Hugo LAMBERT[2], and Geoffrey K. VALLIS[2]

[1]*School of Geography*, *Earth and Environmental Sciences*, *University of Birmingham*, *Birmingham B*15 2*TT*, *UK*

[2]*Department of Mathematics and Statistics*, *University of Exeter*, *Exeter EX*4 4*QJ*, *UK*

[3]*Department of Earth and Environmental Sciences*, *Indian Institute of Science Education and Research*,
Bhopal 462 066, *India*

[4]*School of Ocean and Earth Science, University of Southampton*, *Southampton SO*17 1*BJ*, *UK*

ABSTRACT

The East Asian Summer Monsoon (EASM) provides the majority of annual rainfall to countries in East Asia. Although state-of-the-art models broadly project increased EASM rainfall, the spread of projections is large and simulations of present-day rainfall show significant climatological biases. Systematic evapotranspiration biases occur locally over East Asia, and globally over land, in simulations both with and without a coupled ocean. This study explores the relationship between evapotranspiration and EASM precipitation biases. First, idealized model simulations are presented in which the parameterization of land evaporation is modified, while sea surface temperature is fixed. The results suggest a feedback whereby excessive evapotranspiration over East Asia results in cooling of land, a weakened monsoon low, and a shift of rainfall from the Philippine Sea to China, further fueling evapotranspiration. Cross-model regressions against evapotranspiration over China indicate a similar pattern of behavior in Atmospheric Model Intercomparison Project (AMIP) simulations. Possible causes of this pattern are investigated. The feedback is not explained by an overly intense global hydrological cycle or by differences in radiative processes. Analysis of land-only simulations indicates that evapotranspiration biases are present even when models are forced with prescribed rainfall. These are strengthened when coupled to the atmosphere, suggesting a role for land-model errors in driving atmospheric biases. Coupled atmosphere–ocean models are shown to have similar evapotranspiration biases to those in AMIP over China, but different precipitation biases, including a northward shift in the ITCZ over the Pacific and Atlantic Oceans.

Key words: monsoon, East Asia, China, evapotranspiration, model bias

Article Highlights:

- Idealized model simulations suggest excessive evaporation over China can drive circulation shifts that support further evaporation.
- Similarly, in AMIP, positive evaporation biases over China are correlated with circulation shifts and enhanced precipitation over East Asia.
- Simulations where AMIP land models are forced by prescribed rainfall suggest land parameterizations contribute to the evaporation biases.
- In coupled models, land evaporation biases appear linked to biases in meridional overturning over ocean basins.

---

1. Introduction

East Asian Summer Monsoon (EASM) rainfall is expected to intensify under future climate change (Jin et al., 2020), but the spread of projections in successive Coupled Model Intercomparison Project (CMIP) phases has

remained large. For example, Chen et al. (2020) reported 10th–90th percentile end-of-century rainfall changes varying from 2.63%−25.42% under a high emissions scenario (SSP5-8.5; see O'Neill et al., 2016), or 0.41%−16.31% for low emissions (SSP1-2.6). Confidence in future projections is further reduced by the limitations of climate models, with significant model biases in simulations of present-day monsoon rainfall over Asia and the surrounding oceans (Jiang et al., 2020; Xin et al., 2020).

Identifying the underlying causes of model biases is complicated by bias compensation between model components. In CMIP5, model skill at simulating the EASM was found to benefit from coupling to an ocean versus simulations forced by fixed sea surface temperatures (SSTs) (Song and Zhou, 2014). Yang et al. (2019) showed that models with larger precipitation errors in the atmosphere-only simulations benefited more from coupling to an ocean. They concluded that the coupled models were disguising compensating errors between atmosphere and ocean model components, highlighting the need to examine sources of error in the atmosphere-only and coupled-ocean simulations separately. We find that this bias compensation persists in CMIP6 [Fig. S1 in the electronic supplementary material].

A consistent issue across CMIP phases has been systematic overestimation of evapotranspiration (Mueller and Seneviratne, 2014; Wang et al., 2021), which forms a key component of the atmospheric moisture and moist static energy budgets over land (e.g., Trenberth et al., 2007, 2009). CMIP biases and future change in Asian monsoon rainfall have been shown to relate to energetic contrast between the Northern and Southern Hemispheres, and land–sea thermal contrast (Wang et al., 2020; Chen et al., 2022). In Atmospheric Model Intercomparison Project (AMIP) simulations, SSTs and sea ice are prescribed. Land characteristics, such as hydrology, can then be expected to play a key role in setting land–sea thermal contrast, with land temperatures influenced by availability of soil moisture for evapotranspiration and the consequent partitioning of turbulent fluxes between latent heat and sensible heat (e.g., Seneviratne et al., 2010). Altered land–sea thermal contrast may then induce circulation changes that shift the location of precipitation (cf. Shukla and Mintz, 1982).

For evapotranspiration to occur, two key requirements are availability of soil moisture and evaporative demand from the atmosphere. Where soil moisture is below the wilting point, no evapotranspiration can occur and the surface must warm to balance radiative heating via the sensible heat and longwave radiative fluxes. When soil moisture is sufficiently high it no longer limits evapotranspiration, which is instead influenced by surface temperature and drag, vegetation, and meteorological factors, particularly atmospheric humidity and wind speed (e.g., Seneviratne et al., 2010). Berg and Sheffield (2018) assessed the relationship between soil moisture and evapotranspiration in CMIP5 models by looking at the interannual correlation between the JJA surface soil moisture and latent heat flux at each grid point. Their results show that, although East Asia approaches the demand-limited evapotranspiration regime in both observations and the CMIP5 multimodel mean, it is also a region with significant intermodel variations (see Fig. 2 of Berg and Sheffield, 2018).

Intuition might suggest that enhanced evapotranspiration over a region would chiefly feed back on precipitation by altering moisture recycling within that region. However, model simulations with altered soil moisture or evapotranspiration show that resulting changes in surface temperature can additionally induce geopotential anomalies and dramatically influence the broader atmospheric circulation, including the locations of moisture convergence and precipitation (e.g., Shukla and Mintz, 1982; Agrawal and Chakraborty, 2016; Pietschnig et al., 2021). The EASM region lies between the continental monsoon low, driven by summertime warming of the continent, and the western North Pacific subtropical high (Wang and LinHo, 2002). These circulations converge moisture over East Asia, fueling the monsoon. Rainfall in this region is therefore sensitive to shifts in the interface between these two pressure systems.

Modelling studies investigating the role of soil moisture and evapotranspiration in the Asian monsoon indicate that these affect precipitation via both moisture recycling and advection. Enhanced soil moisture can lead to a strengthening of the monsoon via moisture recycling and enhanced boundary-layer moist static energy, resulting in enhanced convection (Meehl, 1994; Eltahir, 1998). Cooling or warming of the land in response to evapotranspiration alters the circulation and so influences moisture advection (Douville et al., 2001). These effects can alter the range of the Asian monsoon. Chou et al. (2001) found that the monsoon expanded northward in a simulation with saturated soil, with an intensification of rain over East Asia. A number of recent studies have examined the role of soil moisture in interannual variability (Zhang and Zuo, 2011; Gao et al., 2019) and forecasting of EASM rainfall (Zhang and Frederiksen, 2003; Shi et al., 2021), demonstrating a strong influence of local soil moisture anomalies on the monsoon circulation and resultant rainfall, and improved hindcast skill when soil moisture and soil temperature are constrained.

Here, we use idealized model simulations to identify circulation and precipitation patterns that may be introduced by land evaporation biases, and examine the associations between biases in East Asian latent heat flux, circulation and precipitation in AMIP model simulations. Section 2 outlines the datasets and simulations used. In section 3.1 we present idealized model simulations with altered land evaporation. These suggest a feedback whereby excessive land evaporation can maintain a circulation that supports moisture convergence and convection over East Asia, with the resultant precipitation supplying moisture for further evaporation. Section 3.2 presents regressions across AMIP simulations that suggest a similar feedback is present in state-of-the-art models. In section 3.3, we discuss processes that may underlie the AMIP evapotranspiration biases, and show the difference

in behavior in simulations with a coupled ocean. Section 4 summarizes our findings.

2.   Data and methods

2.1.   *Idealized model simulations*

Idealized model simulations are run using the Isca modelling framework (Vallis et al., 2018). The model is based around the GFDL spectral dynamical core (Gordon and Stern, 1982). A wide variety of configurations are available in Isca, but here we use an atmospheric configuration similar to that of Jucker and Gerber (2017). Convection is parameterized via a simple Betts–Miller scheme whereby temperature is relaxed towards a moist adiabat and specific humidity towards a profile with 70% relative humidity, using a 2-h relaxation time for both (Frierson et al., 2006; Frierson, 2007; O'Gorman & Schneider, 2008). Radiation is parameterized using the RRTM scheme, a rapid and accurate multiband radiative transfer model (Mlawer et al., 1997).

The model is run at T42 resolution (~2.8° grid-spacing at the Equator), with 40 vertical sigma-pressure levels. Simulations are designed to have Earth's configuration of continents and orography, with SSTs prescribed to the AMIP climatological mean. An Earth-like obliquity is used (23.439), with no orbital eccentricity. As is common in idealized simulations (e.g., Jucker and Gerber, 2017), clouds are not included, with their role in determining Earth's albedo accounted for via larger ocean and land albedos of 0.25 and 0.325, respectively. While surface temperatures over ocean are prescribed, land temperatures can evolve, with land described as a mixed-layer slab with heat capacity equivalent to 2 m of water. Simulations are run for 50 years, with the first 20 years discarded as spin-up and climatologies taken over the remaining 30 years.

Three simulations are presented, differing only in their description of evaporation over land. In the *bucket* simulation, a simple bucket hydrology is used to describe evapotranspiration (cf. Manabe, 1969; Pietschnig et al., 2019; details in supplementary material), allowing both moisture- and demand-limited regimes to occur. To explore extremes of hydrology, this simulation is compared with two perturbed simulations: (1) *dry-land*, in which land evaporation is set to 0, illustrating a soil moisture–limited regime; and (2) *ocean-land*, in which the same bulk formula is used over land as ocean, i.e., soil is effectively saturated and evaporation is demand-limited.

2.2.   *CMIP6*

We use simulation data from 40 CMIP6 models (Eyring et al., 2016). One ensemble member is used for each model. The models and simulation variant codes used are detailed in Table S1. Data from all models and observational datasets are regridded to a 2.5° grid. This study primarily focuses on the AMIP simulations, in which the atmosphere and land model components are free-running, but SSTs, sea-ice and CO_2 concentrations are prescribed based on observa-

tions. Simulations span the period from 1979 to 2014, but in this study we focus on data from 1980 to 2014 to match the availability of observational data, discussed below. Equivalent data from the atmosphere–ocean coupled simulations with these models are also presented, with the same simulation variant used where possible. We refer to these coupled-ocean simulations as the *historical* simulations, following the CMIP naming convention. Further detail on the AMIP and historical simulations of CMIP6 can be found in Eyring et al. (2016).

In section 3.3, we additionally analyze latent heat flux data from 11 land-only simulations (*land-hist*) from the Land Surface, Snow and Soil moisture Model Intercomparison Project (LS3MIP; van den Hurk et al., 2016). In these simulations, only the land component is run, with climate forcings (land-use, CO_2) prescribed as in the *historical* simulations. The land model is forced with meteorological variables from the Global Soil Wetness Project Phase 3 input dataset (GSWP3; Kim, 2017), which includes prescribed precipitation, wind speed, near-surface air temperature and humidity, surface pressure and downwelling radiative fluxes.

2.3.   *Reanalysis and observations*

Reanalysis and observational data are used to assess the skill of the CMIP6 models in simulating the present-day climatology. Data for geopotential height, 2-m air temperature, evaporation, and zonal, meridional and vertical wind components are taken from JRA-55, which covers the period 1958 onwards (Kobayashi et al., 2015).

In addition to JRA-55, we use land evaporation data from the Global Land Evaporation Amsterdam Model v3.6 (GLEAM; Martens et al., 2017). This combines satellite retrievals of soil moisture, vegetation optical depth, land cover, air temperature and radiation with precipitation and reanalysis data. Data are input to an evapotranspiration model, allowing estimates of actual evaporation and its components to be derived. The output compares well against flux tower measurements from FLUXNET (Martens et al., 2017) and evapotranspiration and soil moisture estimates from other sensors and techniques (Liu et al., 2016; Dembélé et al., 2020; Sriwongsitanon et al., 2020). The GLEAM v3.6 dataset runs from 1980 to 2021. GLEAM is a land dataset; JRA-55 evaporation is used in figures where it is helpful to also show ocean evaporation.

For precipitation, we use the Multi-Source Weighted-Ensemble Precipitation dataset, version 2.8 (MSWEP; Beck et al., 2019). This comprises merged rain gauge, satellite and reanalysis data, and performs well against gauge observations relative to other datasets (Beck et al., 2017). Data are available from 1979 onwards.

Throughout the paper, we use monthly mean climatologies calculated for 1980 to 2014, corresponding to the period of overlap between GLEAM v3.6 and the AMIP simulations.

2.4.   *Cross-model regressions*

We use cross-model linear regressions to summarize rela-

tionships between variables of interest across the AMIP and *historical* model simulations. Specifically, variables are regressed against the following indices: evaporation averaged over land grid points between 110°–120°E and 20°–40°N; global-mean precipitation; and global-mean precipitation over land. As these indices have different magnitudes, all are normalized as:

$$\hat{x}_m = \frac{x_m - \bar{x}}{\sigma_x},$$

where x_m denotes the value of the index in a given model, $\bar{x}$ the multimodel mean, σ_x the cross-model standard deviation, and $\hat{x}_m$ the normalized value for the model.

Regression coefficients are then calculated at each grid point for the mapped variable y as $\sigma_{\hat{x},y}/\sigma_{\hat{x}}^2$. Note that as the normalized standard deviation $\sigma_{\hat{x}} = 1$, this is equivalent to the cross-model covariance of y and the normalized index $\hat{x}$ at each grid point, $\sigma_{\hat{x},y}$.

3. Results

3.1. *Idealized model simulations*

Figure 1 shows the JJA mean climate for each Isca simu-

lation. Differences compared with the *bucket* simulation are shown in Fig. 2. The effects of the altered parameterizations are evident in evaporation over land. In the *dry-land* simulation the evaporative flux is 0 (Fig. 1a), while in *ocean-land* (Fig. 1c) the evaporation over land is similar to that over ocean and exceeds values over the South China Sea and West Pacific, where wind speeds are small. In the *bucket* simulation (Fig. 1b), moderate evaporation occurs over China, the Indochina Peninsula and India, with more limited evaporation over the Tibetan Plateau and negligible evaporation over the Middle East. This distribution of evaporation broadly resembles that in the reanalysis (see Fig. 4, below), although we note that the idealized model is not expected to comprehensively reproduce the observed climate. Over ocean, strong evaporation is co-located with the fastest wind speeds in each simulation.

The altered latent heat flux has a clear impact on surface temperature (Figs. 1d–f). The low heat capacity of land means that it responds quickly to altered surface energy fluxes, and the net surface flux is small. With no clouds, minimal clear-sky absorption, and the same land (0.325) and ocean (0.25) albedo values, the surface shortwave radiative forcing across simulations is approximately identical, and differences between simulations are attributable to the perturbed land evaporation. In the *dry-land* simulation (Fig. 1d), with
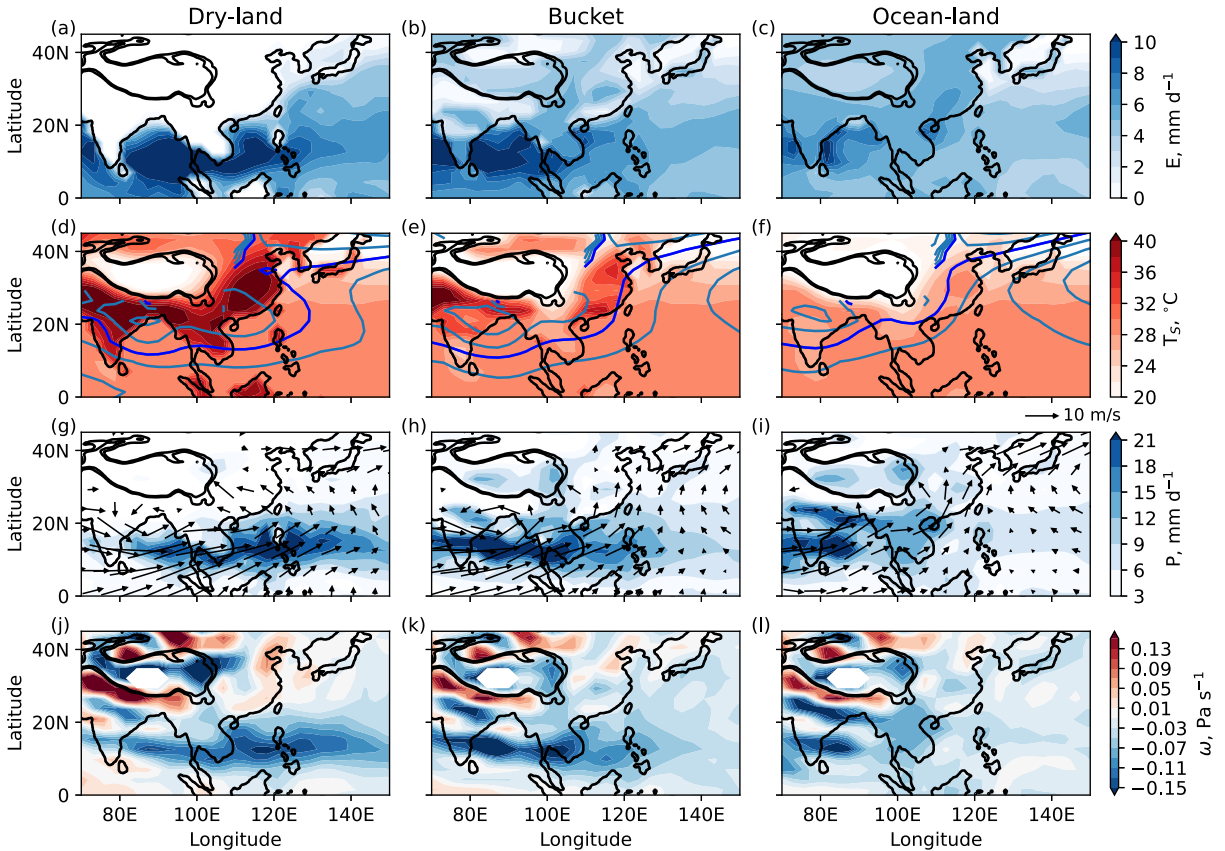

Fig. 1. JJA climatologies for Isca simulations with no evaporation over land (*dry-land*, left), bucket hydrology (*bucket*, center), and ocean-like evaporation over land (*ocean-land*, right). The top row shows evaporation. The second row shows near-surface air temperature (filled contours) and 850-hPa geopotential height (contours; 1350 m in bright blue). The third row shows precipitation (filled contours) and 850-hPa wind (arrows). The bottom row shows 500-hPa ascent, ω.
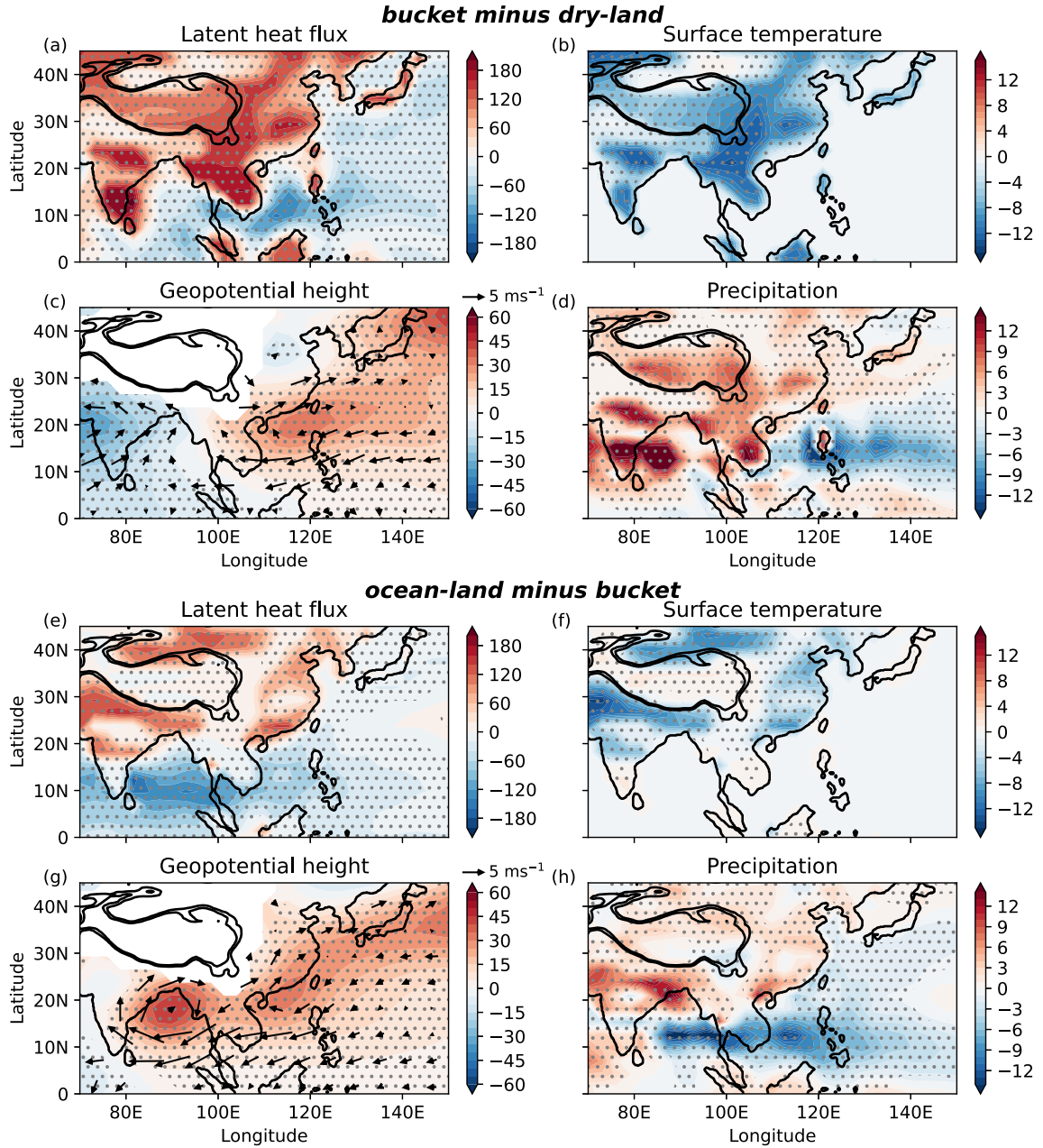
bucket minus dry-land

Fig. 2. Differences between JJA climatological-mean variables. Panels (a–d) show *bucket* minus *dry-land* and (e–h) show *ocean-land* minus *bucket*. Panels show (a, e) latent heat flux (W m^{-2}), (b, f) 2-m air temperature (K), (c, g) 850-hPa geopotential height (m) and 850-hPa wind (m s^{-1}), (d, h) precipitation (mm d^{-1}). Welch's *t*-test is used to assess statistical significance using JJA-mean data for each year. Stippling indicates where differences are statistically different from 0 ($p < 0.05$). Wind vectors are plotted only where windspeed differences are statistically different from 0 ($p < 0.05$). Figure S2 shows *ocean-land* minus *dry-land*.

no land evaporation, the net surface shortwave must be balanced entirely by the sensible heat flux and longwave radiative fluxes. As a result, temperatures over land become warmer than the prescribed SSTs over the neighboring oceans. At the other extreme, in the *ocean-land* simulation (Fig. 1f), evaporation largely balances the shortwave radiative flux, and, except for the regions with high orography, land temperatures are similar to those prescribed over ocean. The *bucket* simulation (Fig. 1e) again provides an intermediate between these two extremes. Here, land-surface temperatures

are generally highest in locations where evaporation is weaker, with the bucket water depth determining the partitioning between latent and sensible heat fluxes.

In the *bucket* simulation, low-level monsoon southwesterlies are seen across the continental coast (Fig. 1h). The Asian continental low meets the western North Pacific subtropical high over the East China and Philippine Seas, and the 850-hPa winds converge and turn northwards over China. The monsoon flow picks up moisture over the Indian and Pacific Oceans (Fig. 1b), and advects it over South and

Southeast Asia and China. In combination with moisture supplied to the boundary layer locally by evaporation, convergence over East Asia drives convection (indicated by mid-level ascent; Fig. 1k) and generates precipitation (Fig. 1h). This in turn replenishes the bucket water depth, maintaining the latent heat flux and land temperature.

The altered land–sea thermal contrast across the simulations drives geopotential anomalies in the atmosphere, and associated circulation and precipitation anomalies. In *dry-land*, the strong thermal gradient between land and ocean is associated with a stronger north–south 850-hPa geopotential gradient over the South China Sea and an eastward-extended geopotential low compared with *bucket* (Figs. 1d and 2c). As a result, the low-level westerly flow across the continental coast is enhanced, particularly over the South China Sea (Figs. 1g and 2c). Strong evaporation occurs over the ocean beneath this flow, but instead of converging moisture over East Asia, these westerlies advect moisture further east, generating intense precipitation over the Philippines (Fig. 1g). In the absence of evaporation to moisten the boundary layer or a supply of moisture from advection, descent occurs over southern and eastern China (Fig. 1j).

In contrast, in *ocean-land*, the north–south thermal contrast and 850-hPa geopotential gradient are reduced over East Asia (Fig. 1f). The westerlies across South and Southeast Asia weaken, and so does ocean evaporation (Figs. 1c, i and 2e–h). The continental low extends less far to the east and the southwesterlies turn north earlier, with only weak wind speeds over the South China Sea compared with the *bucket* or *dry-land* simulations (Figs. 1g–i). Consequently, more moisture is converged over China, and precipitation here is enhanced, while precipitation over the Philippines and South China Sea is reduced (Fig. 2h).

While *dry-land* and *ocean-land* represent limiting cases of land evaporation, the behavior seen in these idealized simulations suggests a possible land–atmosphere feedback that could be present in more realistic simulations. Enhanced evaporation over eastern China could result in cooler land temperatures, leading to reduced thermal and geopotential gradients, and earlier turning of the monsoon flow over East Asia. This altered circulation converges moisture over land in addition to that evaporated locally, fueling convective precipitation and maintaining the supply of moisture for evaporation.

The differences between the idealized simulations (Fig. 2) suggest how the signature of such a feedback might appear in intermodel differences. Key features include: enhanced land evaporation; a high pressure anomaly over the Philippine and East China Seas and North Pacific; enhanced rainfall over land, particularly South and East Asia; and reduced rainfall over the Philippines and Philippine Sea.

3.2. *Evaporation biases in AMIP simulations*

The AMIP simulations show a wide range of behaviors of precipitation and evaporation over East Asia in JJA (Figs. S3–S5 in the electronic supplementary material). The idealized model simulations suggest that an evaporation–circula-

tion–precipitation feedback may influence rainfall over China and the Philippines, and could contribute to model biases in these regions. In this section, we explore whether differences in evapotranspiration across AMIP models are associated with similar circulation and rainfall signals to those seen in the idealized model.

In the idealized simulations, strong differences in evaporation and surface temperature are seen over China when the land evaporation parameterization is varied (Fig. 1). This area showed a diverse range of soil moisture–evaporation coupling across models in CMIP5 (Berg and Sheffield, 2018). To synthesize the range of behaviors in the AMIP simulations, we average the land evaporation over a box corresponding to this strong-signal region (20°–40°N, 110°–120°E) and normalize the value for each model by subtracting the multimodel mean and dividing by the intermodel standard deviation (see section 2.4). We regress other variables against this index describing latent heat flux over China, which we denote CH-LH. Results are not sensitive to the choice of box — for example, similar results are found from regressing against global-mean land evaporation (Fig. S6).

Figure 3 shows cross-model regressions of global fields against CH-LH, which we compare against the idealized simulation differences in Fig. 2. CH-LH is positively correlated with evaporation over non-arid land regions across Asia (Fig. 3a) and globally (Fig. S7), indicating that models with an overly strong CH-LH are likely to have excessive land evaporation elsewhere. Over ocean, relationships are generally weaker and statistically insignificant, with the strongest relationship a negative regression coefficient over the South China Sea, Philippines and western North Pacific.

Stronger CH-LH is associated with cooler 2-m air temperature locally over China (Fig. 3b), as well as over tropical Africa and South America, and northern Eurasia (Fig. S7). The pattern is quite different to the broader continental cooling seen in the idealized model differences (Figs. 2b and f). This difference reflects that, although soils may dry to different degrees across AMIP models, there is still partitioning between latent and sensible heat fluxes, compared with, for example, the *dry-land* simulation where net surface short-wave radiation and temperature are strongly coupled in the absence of evapotranspiration.

The cross-model regressions of 850-hPa geopotential height and precipitation (Figs. 3c and d) show a strikingly similar signal to that seen in the idealized model simulations (Figs. 2c and d). Enhanced CH-LH is correlated with higher geopotential over Southeast Asia and the North Pacific, enhanced precipitation over tropical and midlatitude land, and a deficit of precipitation over the Philippines. We note that these correlations do not necessarily imply the same causal pathway as is forced in the idealized simulations by the experimental design. For example, other processes could drive circulation changes, which then drive the correlations observed. Some alternative hypotheses are explored in section 3.3.

To illustrate the behavior seen in individual models, Fig. 4 compares models with negative (FGOALS-g3) and pos-
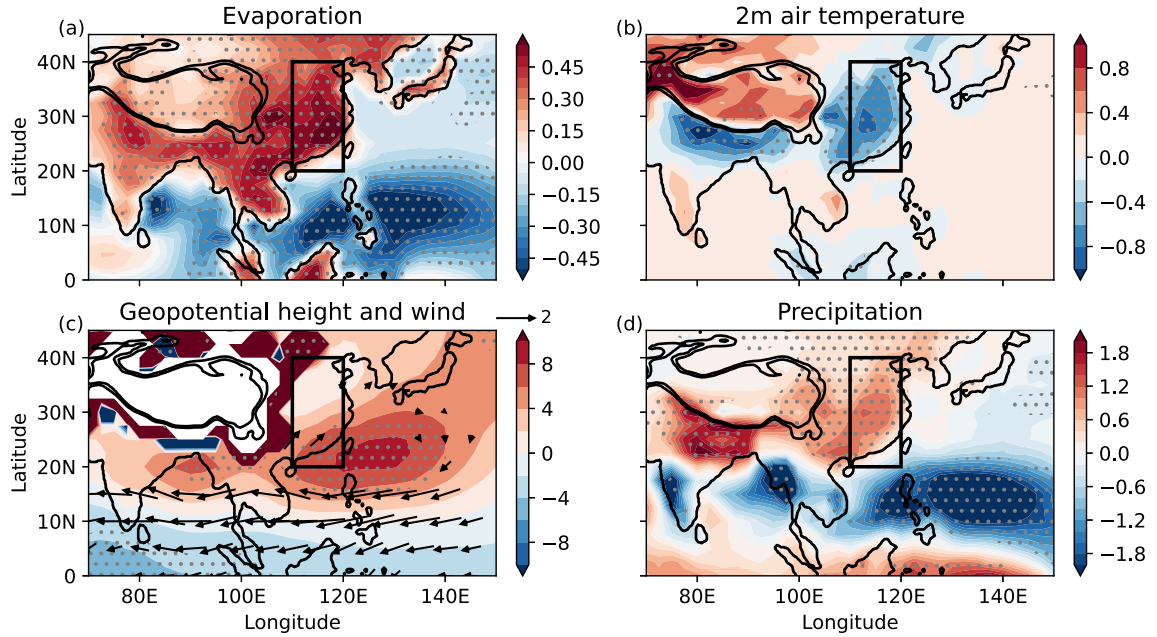
Fig. 3. Cross-model regression of (a) evaporation (mm d^{-1}), (b) 2-m air temperature (K), (c) 850-hPa geopotential height (m) and wind (m s^{-1}), and (d) precipitation (mm d^{-1}) against normalized land evaporation averaged over (20° –40°N, 110°–120°E) ("CH-LH", black box). All data are the JJA climatological-mean in 1980–2014 for the AMIP models listed in Table S1. Stippling indicates where correlations are statistically different from 0 ($p < 0.05$). In panel (c), vectors are plotted only where wind speed correlations against CH-LH are statistically different from 0 ($p < 0.05$). Figure S7 provides the equivalent figure for the full globe.
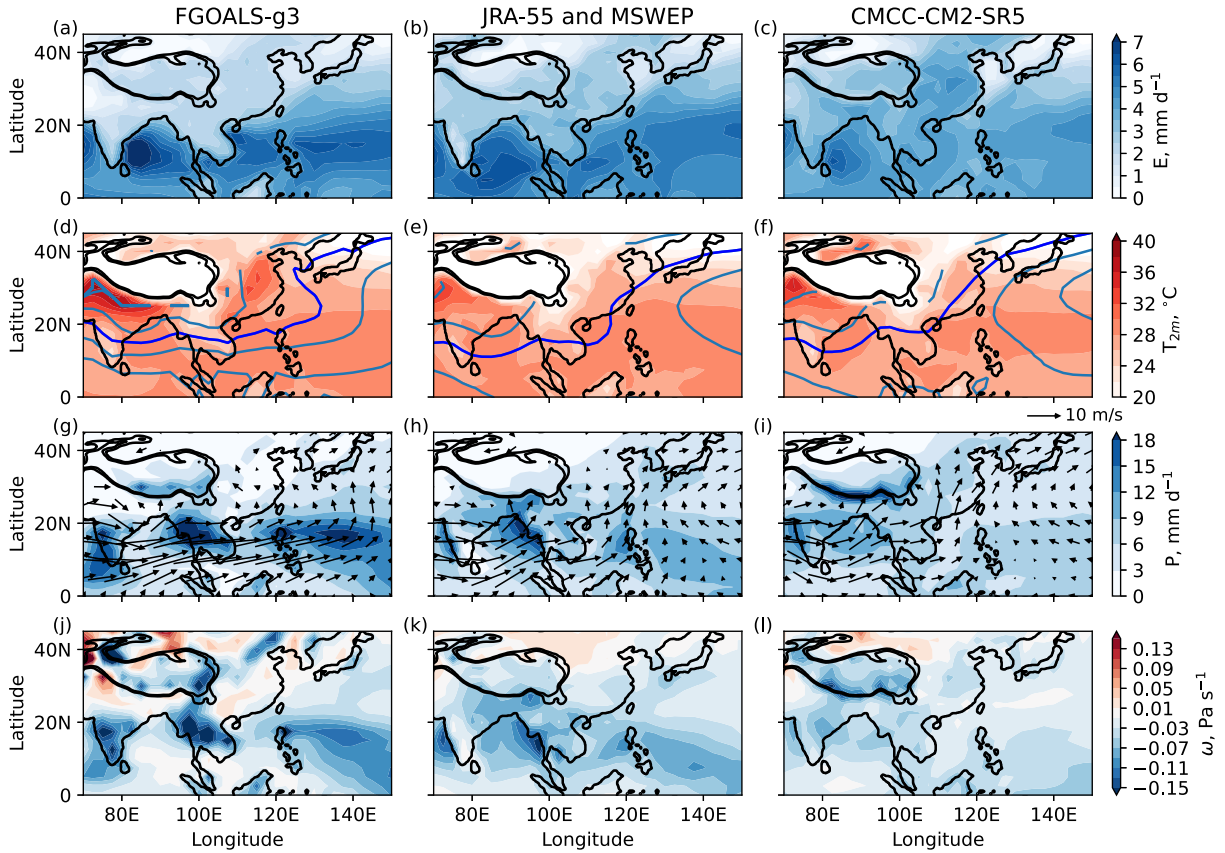

Fig. 4. JJA climatologies for models with deficient (FGOALS-g3, left column) and excessive (CMCC-CM2-SR5, right column) evapotranspiration over East Asia compared with values from observations and reanalysis (MSWEP and JRA-55, center). From top to bottom, rows show evaporation, near-surface air temperature (filled contours) and 850-hPa geopotential height (contours, 1475 m in bright blue), precipitation (filled contours) and 850-hPa wind (arrows), and 500-hPa ascent.

itive (CMCC-CM2-SR5) CH-LH biases against reanalysis and observations. Similar behavior is seen in these individual cases to that in the idealized model simulations (Fig. 1). In FGOALS-g3, where the latent heat flux is weaker, land temperatures are warmer. Similar to the *dry-land* simulation, the monsoon westerlies accelerate under the enhanced geopotential gradient (Fig. 4g). Winds converge to the east of the Philippines, and precipitation falls here, rather than over China, where mid-level descent is observed (Fig. 4j). In CMCC-CM2-SR5, the strong latent heat flux results in cooler air temperatures over China than are seen in JRA-55 and provides a local supply of boundary-layer moisture for convection. The westerlies turn towards southerlies over the Indochina Peninsula and South China Sea, converging additional moisture over China and driving enhanced precipitation and convection (Figs. 4i and l).

The majority of models show excess land evaporation over (20°–40°N, 110°–120°E) compared with observed estimates from GLEAM (38 excess, 2 deficit) and JRA-55 (35 excess, 5 deficit), and the multimodel mean value is 3.4 mm d^{-1} compared with 2.6 mm d^{-1} (GLEAM) and 2.8 mm d^{-1} (JRA-55). The multimodel mean precipitation rate in this region is 5.4 mm d^{-1}, which closely matches observations (MSWEP: 5.4 mm d^{-1}), with wet and dry biased models more evenly spread around the mean. Precipitation and evaporation values in this region are well correlated across models ($r = 0.73$, $p = 7 \times 10^{-8}$). A comparison of values for individual models is provided in Fig. S5. We find that the spatial patterns seen in Fig. 3 remain when the two driest models (FGOALS-g3 and FGOALSf3-L) are excluded from the analysis (Fig. S8), supporting that the signal is not driven by outliers.

3.3. *Roles of atmosphere, land and ocean*

The Isca simulations indicate that similar precipitation shifts to those seen in Fig. 3 can be driven by differences in land evaporation stemming from model parameterization choices. However, in AMIP, multiple processes besides land model errors can influence land–sea contrast and could contribute to the observed behavior; and, as noted above, the correlations observed do not necessarily indicate that evapotranspiration biases are the driver. This section first explores other factors that might contribute to the intermodel differences seen in AMIP — specifically:

- Differences in global hydrological cycle intensity and thus in the availability of soil moisture for evaporation;
- Differences in the demand for land evaporation, e.g., due to clouds and humidity influencing surface temperature and atmospheric moisture demand.

Having explored these alternative hypotheses, we then investigate the potential role of the land parameterizations by examining differences in the behavior of land models when given a specified supply of precipitation and forced with identical atmospheric conditions.

3.3.1. *Effect of hydrological cycle intensity*

The strength of the global hydrological cycle varies across models. For example, in the AMIP simulations presented here, global-mean precipitation rates vary from 2.8 to 3.3 mm d^{-1}. One possible explanation for the global pattern of enhanced/weak land evaporation biases seen in Fig. 3 is that land is wetter and evapotranspiration is stronger in models with a stronger global hydrological cycle.

Figure 5 shows cross-model regressions of the same variables shown in Fig. 3 against the normalized global-mean precipitation for each model. As would be expected from global moisture conservation, evaporation is well correlated with global-mean precipitation across both land and ocean. However, the regional precipitation and geopotential height
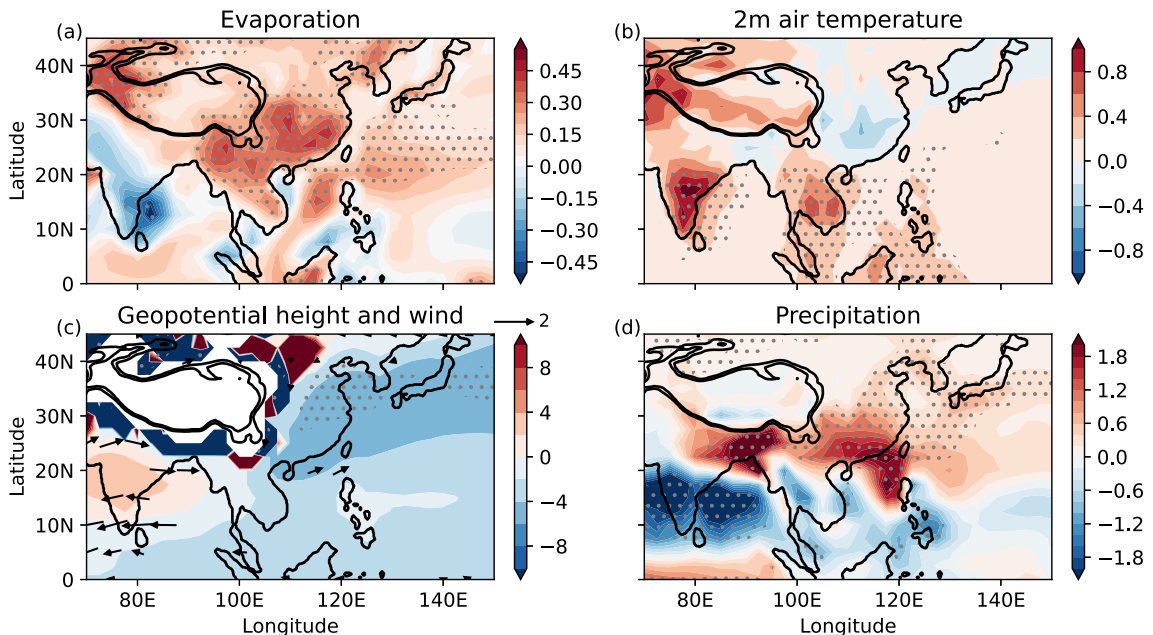

Fig. 5. As Fig. 3 but regressing against normalized global-mean precipitation.

signals seen in Fig. 3 are not evident here, suggesting that intermodel differences in global hydrological cycle strength are not the primary cause of the intermodel differences in land evaporation and the associated temperature, geopotential and precipitation anomalies.

Global land-mean precipitation also varies across AMIP, with a range of 1.6 to 2.7 mm d^{-1} for the simulations used here. Figure 6 shows the regression against normalized global land-mean precipitation. Enhanced land precipitation is positively correlated with land evaporation, and similar geopotential and precipitation signals are seen as in Fig. 3. This is consistent with stronger land precipitation supporting land evaporation anomalies and associated circulation patterns. However, it is not clear whether the enhanced land precipitation arises from circulation biases driven by other processes (e.g., evapotranspiration), or from how convection schemes behave over land in different models.

3.3.2. *Relationship with the surface energy budget*

In addition to the differences in the supply of moisture via hydrological cycle intensity, differences between models could result from biases in evaporative demand. For example, differences in the surface radiation budget relating to clouds or water vapor might enhance or suppress evaporation.

Figure 7 shows terms in the surface energy budget regressed against CH-LH. Land has a low heat capacity, meaning that the net surface energy flux is expected to be small. Consistent with this, an enhanced latent heat flux is correlated with the net downward surface radiative flux over land (Fig. 7a). However, it appears that this is a consequence rather than cause of the enhanced latent heat flux. The net shortwave flux is very weakly correlated with CH-LH over land, with the dominant signal being a positive downward cor-

relation over Southeast Asia and the Philippines (Fig. 7b). This likely relates to the precipitation signal seen in Fig. 3: enhanced evaporation over land is associated with reduced precipitation over the Philippines. This can be expected to reduce cloud cover, and thus generate a positive shortwave anomaly. Looking at the upward and downward longwave fluxes (Figs. 7c and d), it can be seen that enhanced evaporation over China is balanced by reduced upward longwave radiation, with cooler land emitting less longwave radiation. At higher latitudes over Eurasia and North America, a significant correlation is seen with the downward longwave flux, likely due to increased humidity providing a strengthened greenhouse effect.

3.3.3. *Behavior in land-only simulations*

The above subsections have explored possible sources of simulation differences arising from the atmospheric model. Differentiating these from issues arising from the land model is not straightforward. China is a region on the threshold between demand-limited and soil moisture–limited evaporation regimes, with different models simulating each of these states (e.g., Berg and Sheffield, 2018). We found that diagnostics such as the interannual correlation between soil moisture and evaporation (cf. Berg and Sheffield, 2018) or the ratio or difference of evaporation and precipitation (not shown) can inform on which regime individual models are in, but do not allow the underlying driver of the bias to be understood.

To examine whether the land models may contribute to the evaporation biases seen in the AMIP simulations, we use data from 11 land-only model simulations performed for the LS3MIP *land-hist* experiment. Simulations are selected where the land models correspond to that used in the AMIP models presented here. Figure 8a shows the average
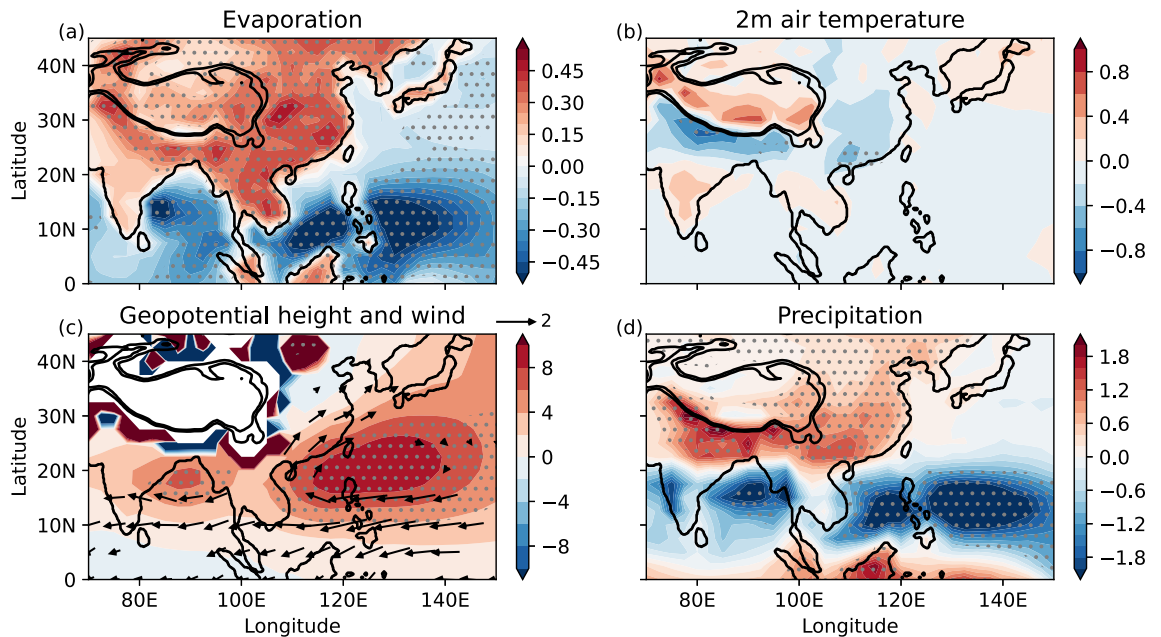

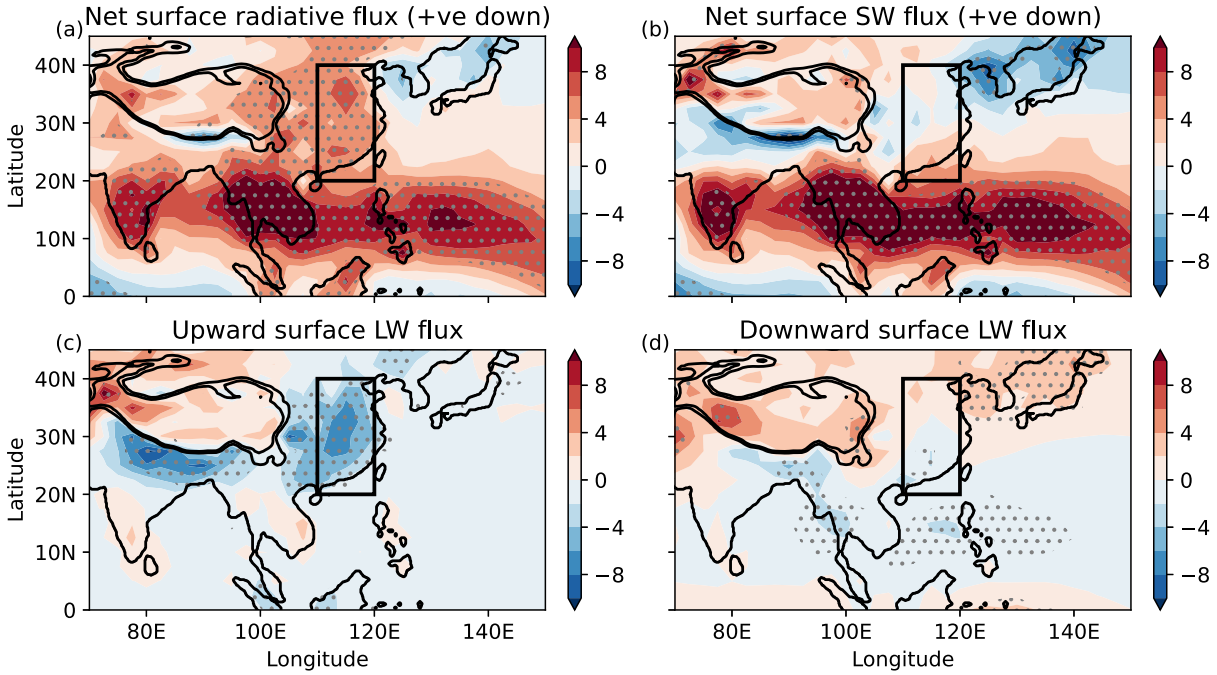**Fig. 6.** As Fig. 3 but regressing against normalized global-mean precipitation over land.

Fig. 7. Cross-model regression of normalized land evaporation averaged over (20°–40°N, 110°–120°E) (black box) with (a) net radiative flux, (b) net surface shortwave flux, (c) upward surface longwave flux, and (d) downward surface longwave flux. Stippling indicates where correlations are statistically different from 0 ($p < 0.05$).
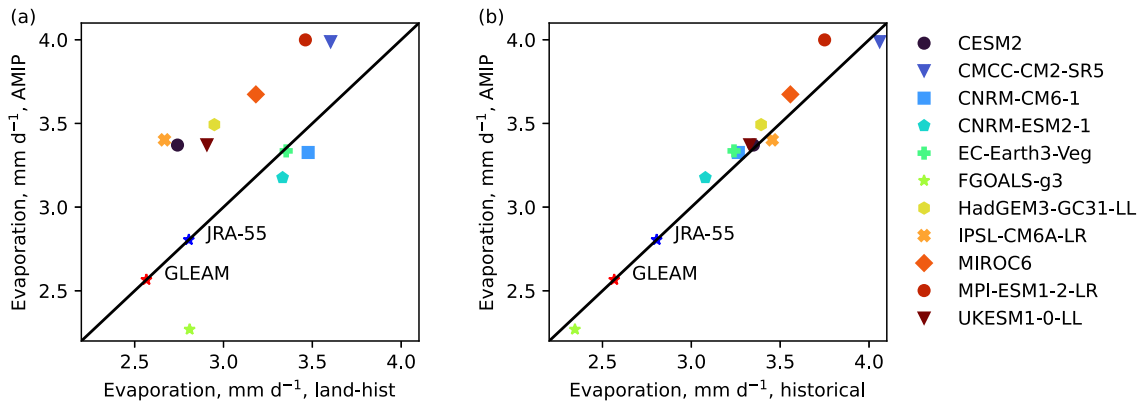

Fig. 8. Average evaporation over China in (a) the AMIP simulations versus equivalent *land-hist* simulations and (b) the AMIP simulations versus equivalent *historical* simulations.

JJA CH-LH in the *land-hist* versus AMIP simulations. Full maps of JJA evaporation relative to GLEAM are shown in Figs. S9–S11 in the electronic supplementary material.

The majority of models simulate excessive evaporation compared to GLEAM and JRA-55 in both the AMIP and *land-hist* simulations. Broadly, models with stronger CH-LH in *land-hist* also have stronger CH-LH in AMIP. The majority of wet-biased models lie above the 1:1 line, indicating that wet biases are enhanced by coupling to the atmosphere. The CNRM models and EC-Earth3-Veg lie close to and slightly below the 1:1 line, suggesting that biases remain in these models but are not amplified with a coupled atmosphere. FGOALS-g3 simulates the closest average evaporation to the observational datasets in *land-hist*, but becomes dry-biased in AMIP.

3.3.4.   *Differences in the coupled-ocean models*

Figure 8b shows the CH-LH in AMIP versus the coupled-ocean *historical* simulations for the subset of models where data are available for *land-hist*. The values are highly correlated ($r = 0.98$, $p = 1×10^{-7}$) and lie close to the 1:1 line. While coupling to an atmosphere tends to exacerbate errors in the land-only simulations (Fig. 8a), coupling the AMIP model to an ocean slightly reduces the difference relative to GLEAM and JRA-55.

Figure 9 shows regressions against CH-LH for the 40 CMIP6 *historical* simulations. Similar to AMIP (Fig. S7), CH-LH is correlated with stronger evaporation over other land regions. A similar but weaker signal of cooler temperatures over China can also be seen, but this relationship is not statistically significant in the *historical* simulations.
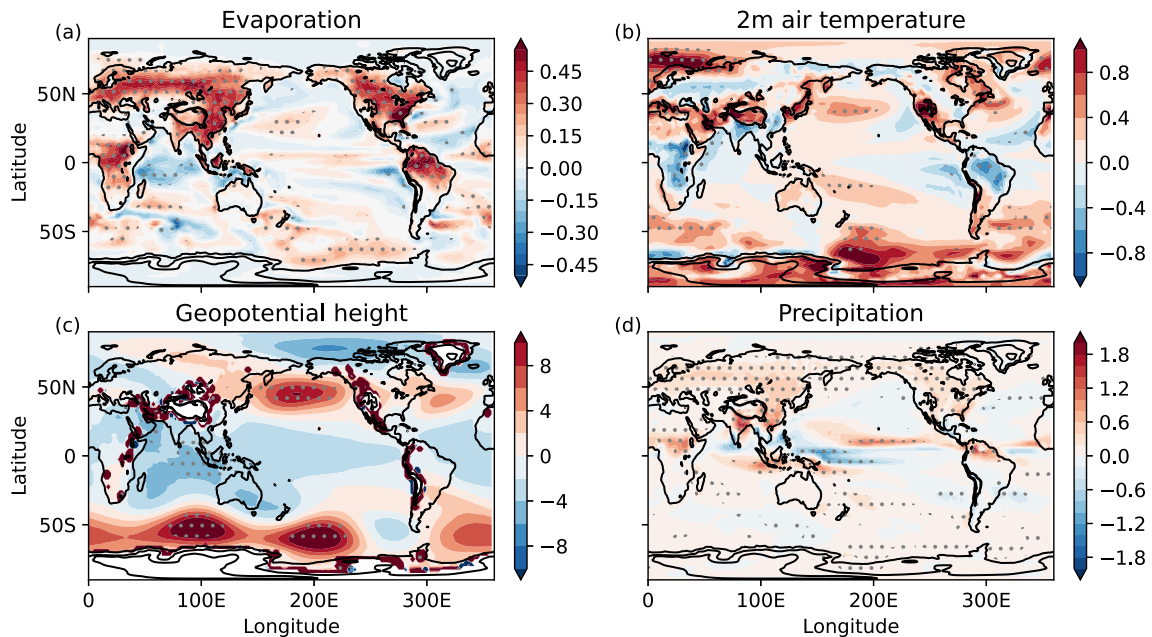
Fig. 9. Cross-model regression of (a) evaporation (mm d^{-1}), (b) 2-m air temperature (K), (c) 850-hPa geopotential height (m), and (d) precipitation (mm d^{-1}) against normalized land evaporation averaged over (20°–40°N, 110°–120° E) ('CH-LH', black box in Fig. 3a). All data are the JJA climatological mean in 1980–2014 for the coupled-ocean *historical* simulations listed in Table S1. Stippling indicates where correlations are statistically different from 0 ($p <$ 0.05).

Clear differences between the AMIP and *historical* simulations are evident in the geopotential and precipitation regressions. The weaker relationship between evaporation and land temperature is reflected in the absence of the geopotential high signal over the East China Sea and the China/Philippines precipitation dipole in the *historical* simulations. Instead, enhanced land evaporation appears associated with a northward shift in the tropical convergence zone (Fig. 9d) over the Pacific and Atlantic.

4.   Conclusions

Idealized model simulations indicate that the positive evapotranspiration biases seen in both CMIP5 and 6 (Mueller and Seneviratne, 2014; Wang et al., 2021) could form part of a self-sustaining feedback, with excessive East Asian summertime evapotranspiration supporting circulation biases associated with excessive precipitation over China and a deficit over the Philippines. This feedback is summarized schematically in Fig. 10. Cross-model regressions in 40 AMIP simulations suggest a relationship between the latent heat flux over China, the low-level circulation and precipitation that is consistent with this feedback.

The idealized simulations demonstrate that variations in the strength of this feedback loop can arise from the parameterization of land hydrology. However, multiple processes could contribute to the behavior in AMIP, and different processes may underlie errors in individual models. Here, we explore three possible aspects that might drive such a feedback loop in AMIP: differences in global hydrological cycle

intensity; errors in surface radiative fluxes – for example, relating to cloud or water vapor; and land model errors. Across models, we find that differences in global hydrological cycle strength or surface radiative fluxes do not appear to explain the evapotranspiration biases, but that land model errors may play a role.

Using data from land-only simulations (*land-hist*), we find that land models show varied evapotranspiration over East Asia, even when driven by the same radiative and meteorological conditions (Fig. 8a). The available *land-hist* data suggest that models with strong evapotranspiration over China in the *land-hist* simulations tend to have further enhanced evapotranspiration when coupled to an atmosphere in the AMIP simulations. This is consistent with excessive evapotranspiration in land-only simulations driving circulation anomalies that converge moisture over China when the land model is coupled to an atmosphere, further amplifying the bias in the land model. It is important to note that other processes besides those explored here could drive the atmospheric circulation biases observed, and thus result in the associated precipitation and evaporation biases.

We highlight that AMIP data alone are not sufficient to identify the root causes of the AMIP precipitation biases. The evapotranspiration regime over East Asia in an individual AMIP simulation may be soil moisture– or demand-limited, and relationships between soil moisture, evaporation, precipitation and runoff can be evaluated that reflect this. However, the evaporative regime is strongly influenced by the amount of precipitation falling over East Asia, which in turn is influenced by pressure and circulation anomalies. The Isca simula-
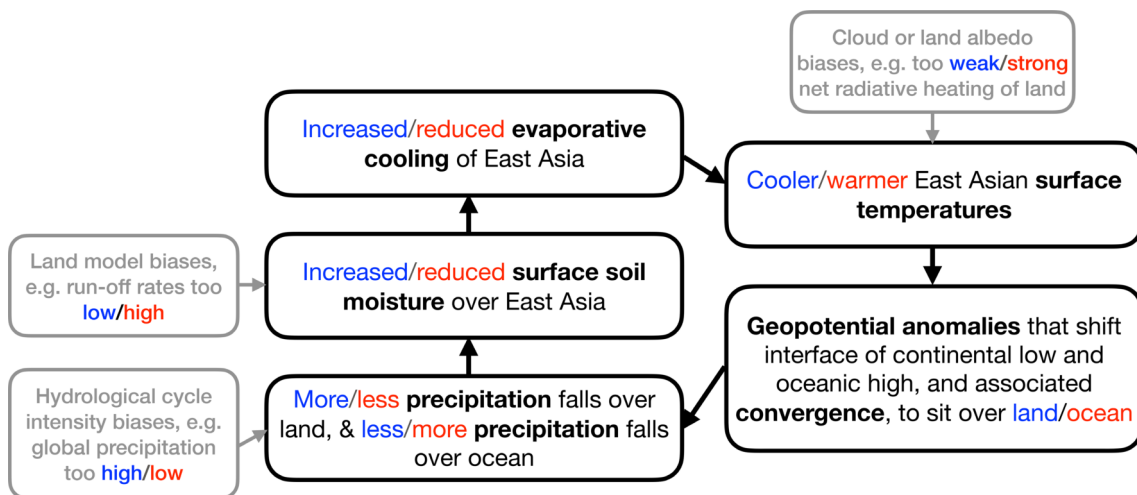
Fig. 10. Schematic illustrating the feedback loop discussed in sections 3.1 and 3.2. Grey boxes show some model biases that might contribute to the feedback, as explored in section 3.3.

tions demonstrate that these, in turn, may be driven by an excess or deficit of evapotranspiration. To identify sources of bias within this loop requires the atmosphere and land model components to be examined separately. Results from only 11 land-only simulations were available for comparison with the AMIP simulations in this study. Greater participation in the *land-hist* simulation would be valuable for untangling these important land–atmosphere interactions.

Evapotranspiration biases over China in the coupled-ocean *historical* simulations are highly correlated with those in AMIP simulations (Fig. 8b). However, the associated circulation and precipitation patterns are very different. The correlation with precipitation over the Philippines seen in AMIP is absent in the coupled models (Fig. 9). This may be explained by the bias compensation mechanism identified by Yang et al. (2019), who found that AMIP models with positive precipitation biases over the northwestern Pacific had a reduced surface energy flux in the same region. When coupled to an ocean, this resulted in a cold SST bias, limiting evaporation and generating pressure and circulation biases that reduced precipitation, compensating for the bias in the atmosphere and land models.

We note that in the coupled-ocean *historical* simulations, excess evaporation over China appears correlated with a slight northward shift of the ITCZ over the Pacific and Atlantic basins. This suggests that while land evaporation biases in fixed-SST simulations influence the circulation primarily by altering stationary wave patterns (e.g., the 850-hPa geopotential height anomalies over East Asia presented here), in coupled simulations the altered land surface energy budget might induce broader scale but weaker shifts in the meridional overturning circulation. Further work and targeted model simulations would be needed to explore this point.

and Associate Editor-in-Chief for their thoughtful and helpful comments on the manuscript.

REFERENCES

Agrawal, S., & A. Chakraborty, 2016: Role of surface hydrology in determining the seasonal cycle of Indian summer monsoon in a general circulation model. *Hydrology and Earth System Sciences Discussions*, in press, https://doi.org/10.5194/hess-2016-591.

Beck, H. E., and Coauthors, 2017: Global-scale evaluation of 22 precipitation datasets using gauge observations and hydrological modeling. *Hydrology and Earth System Sciences*, **21**(12), 6201−6217, https://doi.org/10.5194/hess-21-6201-2017.

Beck, H. E., E. F. Wood, M. Pan, C. K. Fisher, D. G. Miralles, A. I. J. M. van Dijk, T. R. McVicar, and R. F. Adler, 2019: MSWEP V2 Global 3-Hourly 0.1° precipitation: Methodology and quantitative assessment. *Bull. Amer. Meteor. Soc.*, **100**(3), 473−500, https://doi.org/10.1175/BAMS-D-17-0138.1.

Berg, A., and J. Sheffield, 2018: Soil moisture-evapotranspiration

coupling in CMIP5 models: Relationship with simulated climate and projections. *J. Climate*, **31**(12), 4865−4878, https://doi.org/10.1175/JCLI-D-17-0757.1.

Chen, Z. M., T. J. Zhou, L. X. Zhang, X. L. Chen, W. X. Zhang, and J. Jiang, 2020: Global land monsoon precipitation changes in CMIP6 projections. *Geophys. Res. Lett.*, **47**(14), e2019GL086902, https://doi.org/10.1029/2019GL086902.

Chen, Z. M., T. J. Zhou, X. L. Chen, W. X. Zhang, L. X. Zhang, M. N. Wu, and L. W. Zou, 2022: Observationally constrained projection of Afro-Asian monsoon precipitation. *Nature Communications*, **13**(1), 2552, https://doi.org/10.1038/S41467-022-30106-Z.

Chou, C., J. D. Neelin, and H. Su, 2001: Ocean-atmosphere-land feedbacks in an idealized monsoon. *Quart. J. Roy. Meteor. Soc.*, **127**(576), 1869−1891, https://doi.org/10.1002/qj.497 12757602.

Dembélé, M., N. Ceperley, S. J. Zwart, E. Salvadore, G. Mariethoz, and B. Schaefli, 2020: Potential of satellite and reanalysis evaporation datasets for hydrological modelling under various model calibration strategies. *Advances in Water Resources*, **143**, 103667, https://doi.org/10.1016/j.advwatres.2020.103667.

Douville, H., F. Chauvin, and H. Broqua, 2001: Influence of soil moisture on the Asian and African monsoons. Part I: Mean monsoon and daily precipitation. *J. Climate*, **14**(11), 2381−2403, https://doi.org/10.1175/1520-0442(2001)014<2381:IOSMOT>2.0.CO;2.

Eltahir, E. A. B., 1998: A soil moisture-rainfall feedback mechanism: 1. Theory and observations. *Water Resour. Res.*, **34**(4), 765−776, https://doi.org/10.1029/97WR03499.

Eyring, V., S. Bony, G. A. Meehl, C. A. Senior, B. Stevens, R. J. Stouffer, and K. E. Taylor, 2016: Overview of the Coupled Model Intercomparison Project Phase 6 (CMIP6) experimental design and organization. *Geoscientific Model Development*, **9**(5), 1937−1958, https://doi.org/10.5194/gmd-9-1937-2016.

Frierson, D. M. W., 2007: The dynamics of idealized convection schemes and their effect on the zonally averaged tropical circulation. *J. Atmos. Sci.*, **64**(6), 1959−1976, https://doi.org/10.1175/JAS3935.1.

Frierson, D. M. W., I. M. Held, and P. Zurita-Gotor, 2006: A gray-radiation aquaplanet moist GCM. Part I: Static stability and eddy scale. *J. Atmos. Sci.*, **63**(10), 2548−2566, https://doi.org/10.1175/JAS3753.1.

Gao, C. J., and Coauthors, 2019: Land-atmosphere interaction over the Indo-China Peninsula during spring and its effect on the following summer climate over the Yangtze River basin. *Climate Dyn.*, **53**(9−10), 6181−6198, https://doi.org/10.1007/s00382-019-04922-x.

Gordon, C. T., and W. F. Stern, 1982: A description of the GFDL global spectral model. *Mon. Wea. Rev.*, **110**(7), 625−644, https://doi.org/10.1175/1520-0493(1982)110<0625:ADOTGG>2.0.CO;2.

Jiang, D. B., D. Hu, Z. P. Tian, and X. M. Lang, 2020: Differences between CMIP6 and CMIP5 models in simulating climate over China and the East Asian monsoon. *Adv. Atmos. Sci.*, **37**(10), 1102−1118, https://doi.org/10.1007/s00376-020-20 34-y.

Jin, C. H., B. Wang, and J. Liu, 2020: Future changes and controlling factors of the eight regional monsoons projected by CMIP6 models. *J. Climate*, **33**(21), 9307−9326, https://doi.org/10.1175/JCLI-D-20-0236.1.

Jucker, M., and E. P. Gerber, 2017: Untangling the annual cycle of the tropical tropopause layer with an idealized moist model. *J. Climate*, **30**(18), 7339−7358, https://doi.org/10.1175/JCLI-D-17-0127.1.

Kim, H., 2017: Global soil wetness project phase 3 atmospheric boundary conditions (experiment 1) [data set], data integration and analysis system (DIAS). https://doi.org/10.20783/DIAS.501.

Kobayashi, S., and Coauthors, 2015: The JRA-55 reanalysis: General specifications and basic characteristics. *J. Meteor. Soc. Japan*, **93**(1), 5−48, https://doi.org/10.2151/jmsj.2015-001.

Liu, W. B., L. Wang, J. Zhou, Y. Z. Li, F. B. Sun, G. B. Fu, X. P. Li, and Y.-F. Sang, 2016: A worldwide evaluation of basin-scale evapotranspiration estimates against the water balance method. *J. Hydrol.*, **538**, 82−95, https://doi.org/10.1016/j.jhydrol.2016.04.006.

Manabe, S., 1969: Climate and the Ocean Circulation: 1. The atmospheric circulation and the hydrology of the earth's surface. *Mon. Wea. Rev.*, **97**(11), 739−774, https://doi.org/10.1175/1520-0493(1969)097<0739:CATOC>2.3.CO;2.

Martens, B., and Coauthors, 2017: GLEAM v3: Satellite-based land evaporation and root-zone soil moisture. *Geoscientific Model Development*, **10**(5), 1903−1925, https://doi.org/10.5194/gmd-10-1903-2017.

Meehl, G. A., 1994: Influence of the land surface in the Asian summer monsoon: External conditions versus internal feedbacks. *J. Climate*, **7**(7), 1033−1049, https://doi.org/10.1175/1520-0442(1994)007<1033:IOTLSI>2.0.CO;2.

Mlawer, E. J., S. J. Taubman, P. D. Brown, M. J. Iacono, and S. A. Clough, 1997: Radiative transfer for inhomogeneous atmospheres: RRTM, a validated correlated-k model for the longwave. *J. Geophys. Res.*, **102**(D14), 16 663−16 682, https://doi.org/10.1029/97JD00237.

Mueller, B., and S. I. Seneviratne, 2014: Systematic land climate and evapotranspiration biases in CMIP5 simulations. *Geophys. Res. Lett.*, **41**(1), 128−134, https://doi.org/10.1002/2013GL058055.

O'Gorman, P. A., and T. Schneider, 2008: The hydrological cycle over a wide range of climates simulated with an idealized GCM. *J. Climate*, **21**, 3815−3832, https://doi.org/10.1175/2007JCLI2065.1.

O'Neill, B. C., and Coauthors, 2016: The scenario model intercomparison project (ScenarioMIP) for CMIP6. *Geoscientific Model Development*, **9**(9), 3461−3482, https://doi.org/10.5194/gmd-9-3461-2016.

Pietschnig, M., F. H. Lambert, M. Saint-Lu, and G. K. Vallis, 2019: The presence of Africa and limited soil moisture contribute to future drying of South America. *Geophys. Res. Lett.*, **46**(21), 12 445−12 453, https://doi.org/10.1029/2019GL084441.

Pietschnig, M., A. L. S. Swann, F. H. Lambert, and G. K. Vallis, 2021: Response of tropical rainfall to reduced evapotranspiration depends on continental extent. *J. Climate*, **34**(23), 9221−9234, https://doi.org/10.1175/JCLI-D-21-0195.1.

Seneviratne, S. I., T. Corti, E. L. Davin, M. Hirschi, E. B. Jaeger, I. Lehner, B. Orlowsky, and A. J. Teuling, 2010: Investigating soil moisture-climate interactions in a changing climate: A review. *Earth-Science Reviews*, **99**(3−4), 125−161, https://doi.org/10.1016/j.earscirev.2010.02.004.

Shi, P. F., and Coauthors, 2021: Significant land contributions to interannual predictability of East Asian summer monsoon rainfall. *Earth's Future*, **9**(2), e2020EF001762, https://doi.org/

10.1029/2020EF001762.

Shukla, J., and Y. Mintz, 1982: Influence of land-surface evapotran-spiration on the earth's climate. *Science*, **215**(4539), 1498−1501, https://doi.org/10.1126/science.215.4539.1498.

Song, F. F., and T. J. Zhou, 2014: The climatology and interannual variability of East Asian summer monsoon in CMIP5 coupled models: Does air-sea coupling improve the simulations. *J. Climate*, **27**(23), 8761−8777, https://doi.org/10.1175/JCLI-D-14-00396.1.

Sriwongsitanon, N., T. Suwawong, S. Thianpopirug, J. Williams, L. Jia, and W. Bastiaanssen, 2020: Validation of seven global remotely sensed ET products across Thailand using water balance measurements and land use classifications. *J. Hydrol.*, **30**, 100709, https://doi.org/10.1016/j.ejrh.2020.100709.

Trenberth, K. E., J. T. Fasullo, and J. Kiehl, 2009: Earth's global energy budget. *Bull. Amer. Meteor. Soc.*, **90**(3), 311−324, https://doi.org/10.1175/2008BAMS2634.1.

Trenberth, K. E., L. Smith, T. T. Qian, A. G. Dai, and J. Fasullo, 2007: Estimates of the global water budget and its annual cycle using observational and model data. *Journal of Hydrometeorology*, **8**(4), 758−769, https://doi.org/10.1175/JHM600.1.

Vallis, G. K., and Coauthors, 2018: Isca, v1.0: a framework for the global modelling of the atmospheres of Earth and other planets at varying levels of complexity. *Geoscientific Model Development*, **11**(3), 843−859, https://doi.org/10.5194/gmd-11-843-2018.

van den Hurk, B., and Coauthors, 2016: LS3MIP (v1.0) contribution to CMIP6: The Land Surface, Snow and Soil moisture Model Intercomparison Project - aims, setup and expected outcome. *Geoscientific Model Development*, **9**(8), 2809−2832, https://doi.org/10.5194/gmd-9-2809-2016.

Wang, B., and LinHo, 2002: Rainy season of the Asian-Pacific summer monsoon. *J. Climate*, **15**(4), 386−398, https://doi.org/10.1175/1520-0442(2002)015<0386:RSOTAP>2.0.CO;2.

Wang, B., C. Jin, and J. Liu, 2020: Understanding future change of global monsoons projected by CMIP6 models. *J. Climate*, **33**(15), 6471−6489, https://doi.org/10.1175/JCLI-D-19-0993.1.

Wang, Z. Z., C. S. Zhan, L. K. Ning, and H. Guo, 2021: Evaluation of global terrestrial evapotranspiration in CMIP6 models. *Theor. Appl. Climatol.*, **143**(1), 521−531, https://doi.org/10.1007/s00704-020-03437-4.

Xin, X. G., T. W. Wu, J. Zhang, J. C. Yao, and Y. J. Fang, 2020: Comparison of CMIP6 and CMIP5 simulations of precipitation in China and the East Asian summer monsoon. *International Journal of Climatology*, **40**(15), 6423−6440, https://doi.org/10.1002/joc.6590.

Yang, B., and Coauthors, 2019: Better monsoon precipitation in coupled climate models due to bias compensation. *npj Climate and Atmospheric Science*, **2**(1), 43, https://doi.org/10.1038/s41612-019-0100-x.

Zhang, H., and C. S. Frederiksen, 2003: Local and nonlocal impacts of soil moisture initialization on AGCM seasonal forecasts: A model sensitivity study. *J. Climate*, **16**(13), 2117−2137, https://doi.org/10.1175/1520-0442(2003)16<2117:LANIOS>2.0.CO;2.

Zhang, R. H., and Z. Y. Zuo, 2011: Impact of spring soil moisture on surface energy balance and summer monsoon circulation over East Asia and precipitation in East China. *J. Climate*, **24**(13), 3309−3322, https://doi.org/10.1175/2011JCLI4084.1.